JACS
JOURNAL OF THE AMERICAN CHEMICAL SOCIETY

ARTICLE

pubs.acs.org/JACS

Matrix Gla Protein Inhibits Ectopic Calcification by a Direct Interaction with Hydroxyapatite Crystals

Jason O'Young,[†] Yinyin Liao,[†] Yizhi Xiao,[†] Jari Jalkanen,[‡] Gilles Lajoie,[∥] Mikko Karttunen,[‡,§] Harvey A. Goldberg,[†,∥] and Graeme K. Hunter*[,†,∥]

[†]School of Dentistry, [‡]Department of Applied Mathematics, and [∥]Department of Biochemistry, University of Western Ontario, London, Canada

Supporting Information Web-Enhanced

ABSTRACT: Mice lacking the gene encoding matrix gla protein (MGP) exhibit massive mineral deposition in blood vessels and die soon after birth. We hypothesize that MGP prevents arterial calcification by adsorbing to growing hydroxyapatite (HA) crystals. To test this, we have used a combined experimental−computational approach. We synthesized peptides covering the entire sequence of human MGP, which contains three sites of serine phosphorylation and five sites of γ-carboxylation, and studied their effects on HA crystal growth using a constant-composition autotitration assay. In parallel studies, the interactions of these sequences with the {100} and {001} faces of HA were analyzed using atomistic molecular dynamics (MD) simulations. YGlapS (amino acids 1−14 of human MGP) and SK-Gla (MGP43−56) adsorbed rapidly to the {100} and {001} faces and strongly inhibited HA growth (IC_{50} = 2.96 μg/mL and 4.96 μg/mL, respectively). QR-Gla (MGP29−42) adsorbed more slowly and was a moderate growth inhibitor, while the remaining three (nonpost-translationally modified) peptides had little or no effect in either analysis. Substitution of gla with glutamic acid reduced the adsorption and inhibition activities of SK-Gla and (to a lesser extent) QR-Gla but not YGlapS; substitution of phosphoserine with serine reduced the inhibitory potency of YGlapS. These studies suggest that MGP prevents arterial calcification by a direct interaction with HA crystals that involves both phosphate groups and gla residues of the protein. The strong correlation between simulated adsorption and measured growth inhibition indicates that MD provides a powerful tool to predict the effects of proteins and peptides on crystal formation.

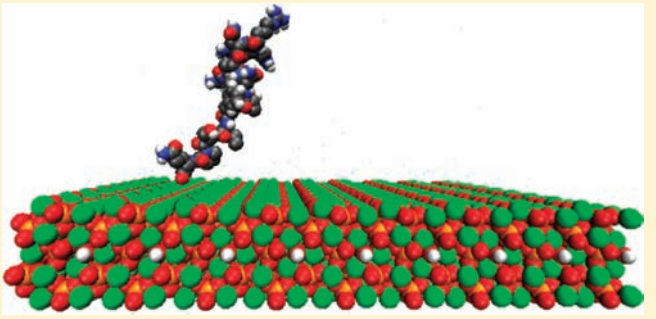

INTRODUCTION

Interactions between proteins and biological crystals are believed to play a central role not only in determining the location, type, orientation, and growth habit (size and shape) of crystals in tissues such as bones, teeth, and shells but also in preventing or limiting mineral formation in soft tissues.[1−3] The chemistry of this unique organic−inorganic interface, composed of crystal surfaces containing a variety of lattice ions and substituents, steps and other lattice dislocations, its associated water and counterion layers, and complex protein structures with a wide range of functional groups, is still poorly understood. However, the elucidation of protein−biomineral interactions holds the promise of developing therapies for common diseases, tissue-engineering mineralized tissues, and designing materials with novel properties.

Biological fluids such as blood, saliva, urine, and interstitial fluids are supersaturated but metastable with respect to a variety of mineral phases, including calcium phosphates and calcium oxalates. Therefore, a critical crystal nucleus forming in a tissue or fluid can grow and propagate indefinitely. This process can give rise to medically important ectopic calcifications such as kidney stones, atherosclerotic plaque, and dental calculus.[4]

Calcification of soft tissues and biological fluids is limited by the presence of high and low molecular weight inhibitors.[5] The latter include pyrophosphate[6] and citrate;[7] the former are mainly proteins.[8] The identification of proteins as inhibitors of calcification is made on a variety of criteria, most based on in vitro studies, but the most definitive criterion is that genetic ablation of that protein in experimental animals results in soft-tissue calcification.

Perhaps the most dramatic calcification phenotype results from deletion of the gene coding for matrix gla protein (MGP). Mice homozygous for an MGP-null mutation die a few weeks after birth of arterial rupture. Histology of the major vessels of these animals reveals extensive deposition of mineral between the elastic laminae of the intima. The growth plate cartilage of MGP knockout mice is also hypermineralized.[9] Although MGP circulates in the blood,[10] the MGP-null phenotype is not rescued by overexpression of the protein by liver cells. However, it is

Received: August 12, 2011
Published: September 30, 2011

Table 1. Summary of Crystal Growth and Molecular Dynamics Data

peptide name	amino acid nos.	sequence	[a]crystal growth rate (μL/min)	[b]mean peptide-{100} face distance (nm)	[b]rmsd (nm)
–	–	–	4.07 ± 0.002	–	–
YGlapS	1–14	YγEpSHEpSMEpSYELNP	0	0.683	0.017
YEpS	1–14	YEpSHEpSMEpSYELNP	0	0.770	0.018
YGlaS	1–14	YγESHESMESYELNP	2.11 ± 0.011	0.815	0.022
YES	1–14	YESHESMESYELNP	2.44 ± 0.008	0.764	0.027
FIN	15–28	FINRRNANTFISPQ	3.74 ± 0.003	1.90	0.166
QR-Gla	29–42	QRWRAKVQγERIRγER	3.05 ± 0.006	0.991	0.078
QRE	29–42	QRWRAKVQERIRER	3.76 ± 0.007	1.47	0.182
SK-Gla	43–56	SKPVHγELNRγEACDD	0	0.917	0.045
SKE	43–56	SKPVHELNREACDD	2.16 ± 0.011	1.21	0.138
YRL	57–70	YRLCERYAMVYGYN	4.74 ± 0.002	4.25	0.740
AAY	71–84	AAYNRYFRKRRGTK	4.16 ± 0.004	3.63	0.389

[a] Calculated from the data shown in Figures 1A and S1 of the Supporting Information [b] Calculated from the data shown in Figure 2A.

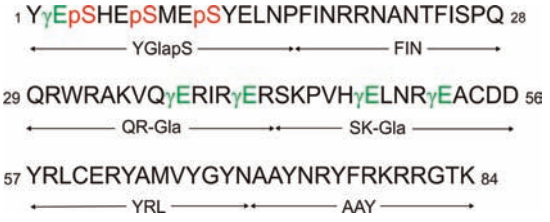

Figure 1. Amino acid sequences of human MGP and peptides used in the present study. γE = γ-carboxyglutamic acid (gla); pS = phosphoserine.

rescued by overexpression of MGP in vascular smooth muscle cells.[11] Thus, MGP is believed to function as a local inhibitor of blood vessel calcification.

There are also findings that suggest a link between MGP and ectopic calcification in humans. Mutations in the MGP gene have been shown to be the cause of Keutel syndrome,[12,13] which is characterized in part by hypermineralization of cartilage. Keutel patients also suffer from calcification of a number of arteries.[14] Polymorphisms in the MGP gene have been correlated with the incidences of coronary artery calcification[15] and kidney stone disease.[16]

Human MGP is an 84 amino acid protein containing 5 γ-carboxyglutamic acid (gla) residues.[17] Three sites of serine phosphorylation, all close to the N-terminus, have been identified in MGP from human and other mammals. The levels of phosphorylation of serines 3, 6, and 9 in human MGP were reported to be 87, 83, and 92%, respectively.[18] Nonphosphorylated synthetic human MGP has been shown to contain ~21% α helix, a proportion that is increased in the presence of Ca^{2+} ions.[19] No information is available on the tertiary structure of MGP, apparently because the protein is poorly soluble.[20]

Studies with the vitamin K antagonist warfarin suggest that γ-carboxylation is required for the anticalcification activities of MGP. Treatment of rats with warfarin results in excessive mineralization of growth plate cartilage[21] and a pattern of vascular calcification similar to that seen in the MGP-null mouse.[22] Both effects can be attributed to MGP rather than osteocalcin or other gla-containing proteins.[22,23] In vitro, warfarin increases the calcification of vascular smooth muscle cells[24] and hypertrophic chondrocytes.[25]

Based on present knowledge, there are two mechanisms by which MGP could inhibit the calcification of blood vessels and cartilage. The first is a direct interaction between the protein and nascent crystals, as has been shown for osteocalcin as well as a variety of phosphoproteins and phosphopeptides.[26−28] It is quite plausible that the gla and phosphate groups, as well as other acidic residues, could allow MGP to adsorb to crystals and thereby limit or prevent lattice ion addition to crystals. A moderate affinity interaction between MGP and hydroxyapatite (HA) has been reported.[29] Of possible relevance is the finding of a complex containing MGP, fetuin, and calcium phosphate in the serum of bisphosphonate-treated rats.[30]

The second plausible mechanism by which MGP could prevent soft tissue calcification is by inhibition of cellular differentiation. Atherosclerosis is now understood to be an active process in which the arterial wall transforms into a tissue very similar to bone.[31] Because it acts as an antagonist of bone morphogenetic protein 2, MGP can inhibit osteogenesis.[32]

The object of the present study was to determine whether MGP inhibits the formation of HA crystals. Using a combination of computational (molecular dynamics) and experimental (autotitration) techniques, we demonstrate that peptides based on sequences in human MGP adsorb to and inhibit the growth of HA. These activities are highly dependent on both γ-carboxylation and phosphorylation of the protein.

EXPERIMENTAL SECTION

Peptide Synthesis. The MGP peptides used in this study are listed in Table 1. Their positions within the protein sequence are shown in Figure 1. Phosphorylated non-γ-carboxylated peptides were synthesized using Fmoc (9-fluorenylmethyloxycarbonyl) chemistry as previously described.[33,34] γ-Carboxylated peptides as well as all other peptides were purchased from American Peptide Company. All peptides were purified by high performance liquid chromatography (HPLC) to achieve >95% purity and verified by mass spectrometry.

Constant-Composition Seeded Growth Analysis of HA Crystal Growth. Titrations were carried out as described in ref 34. In brief, HA seed crystals (2 mg) were added to 8 mL of a solution supersaturated with respect to HA and maintained at 37 °C. Using a Radiometer Titration Manager and Triburet, titrants were added to the crystal suspension to maintain a constant pH of 7.4 and constant concentrations of Ca^{2+} (0.5 mM), phosphate (0.3 mM), and NaCl

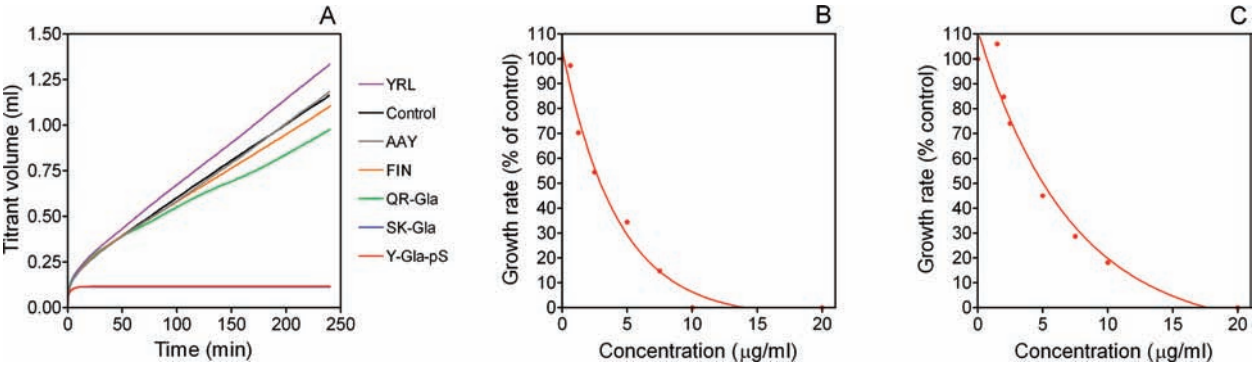

Figure 2. Effect of MGP peptides on seeded growth of HA. (A) Native peptides, 20 μg/mL; (B) YGlapS; (C) SK-Gla.

(150 mM). Crystal growth rates were calculated by linear regression of plots of titrant volume added against time over the period 20−240 min.

MD Simulations of MGP Peptide−HA Adsorption. Atomic-level MD simulations were performed using GROMACS, release 3.3.3[35] with GROMOS96 force field, version 45A3.[36] The parameters for the bond lengths, angles, and dihedral angles of the two side chain COO^- groups in gla were the same as those of the single COO^- group in a glu residue. The parameters controlling the angle between the COO^--groups and the γ-carbon were set to the generic value used by the force-field between two CH groups in the side-chain backbone.

The HA crystal faces {100} and {001} were created as described in ref 34. The size of the simulation cell was 10 nm perpendicular to the surface. The planar dimensions were 8.4 nm × 6.2 nm for the {100} and 9.7 nm × 6.6 nm for the {001} case. Periodic boundary conditions were applied. The peptides were placed ∼5 nm above the crystal at the beginning of the simulations. The system was solvated with simple point charge (SPC) water,[37] which works reliably with the GROMOS96 force field.[38] Cl^- counterions were added to maintain the system charge-neutral. There were totals of approximately 49 400 and 61 400 atoms in the systems with the HA {100} and {001} faces, respectively.

The bond lengths were constrained using the SHAKE algorithm,[39] and the crystal atoms were constrained to their equilibrium positions. The simulations were performed in the NVT (constant particle number, volume, and temperature) ensemble at T = 300 K. The weak coupling thermostat with a coupling time constant of 0.1 ps was employed. A cutoff of 1.0 nm was used for both Lennard−Jones interactions and the real space part of the particle mesh Ewald method for electrostatics.[40,41] Since electrostatics is one of the major driving forces here, it is crucial to treat it explicitly and to keep charge groups small to avoid spurious artifacts.[42−44] The time step was set to 2 fs, and the total simulation time was 20 ns.

Statistical Analysis. HA growth rates were calculated by linear regression of constant-composition data (titrant volume versus time) over the period 20−240 min. Growth rates were plotted against peptide concentration and fitted to one-phase exponential decay curves. The IC_{50} values quoted represent the half-lives of the decay curves.

For MD studies, positions of peptide and side-chain centers of mass were calculated by averaging out the positions of all atoms involved. Distances along the z-axis of the simulation box between the centers of mass and the outermost layer of crystal atoms were measured. Finally, the means and standard deviations of these values were calculated over the period 10−20 ns.

RESULTS

Inhibition of HA Growth by MGP Peptides. Six peptides, corresponding to contiguous 14 amino acid sequences of human MGP, were synthesized (see Figure 1). One of these, YGlapS, contains the three phosphate groups and one gla residue. Two of the peptides, QR-Gla and SK-Gla, each contain two gla residues. The remaining three peptides, FIN, YRL, and AAY, contain no known sites of post-translational modification. To study the role of γ-carboxylation in MGP function, additional peptides that have glutamic acid (glu) residues instead of gla (YEpS, QR-E, and SK-E) were synthesized. To study the role of phosphorylation, peptides that have serine residues instead of phosphoserine (YGlaS and YES) were synthesized.

Inhibition of HA crystal growth by MGP peptides was studied using a constant-composition seeded-growth method. In this assay, initial growth is exponential, but subsequent growth is linear.[34] Therefore, growth rates were calculated using data from 20 to 240 min of incubation.

Initially, the effect of each of the six "native" peptides on HA crystal growth was studied at 20 μg/mL. YGlapS and SK-Gla were most potent, causing essentially complete inhibition of growth. QR-Gla had lesser inhibitory activity, reducing the growth rate by ∼25%, while the remaining three (nonpost-translationally modified) peptides had little or no effect (Figure 2A). (Interestingly, YRL somewhat increased the rate of crystal growth.) The effects of YGlapS and SK-Gla were examined in more detail by using a range of peptide concentrations in the constant-composition assay. Plots of growth rate against inhibitor concentration were analyzed by nonlinear regression to produce IC_{50} values of 2.96 μg/mL for YGlapS and 4.96 μg/mL for SK-Gla (Figure 2B,C).

The effects of γ-carboxylation are shown in the Supporting Information, Figure S1A. Whereas 20 μg/mL SK-Gla caused complete inhibition of crystal growth, SK-E caused only 47% inhibition. A similar relative difference was observed between QR-Gla (25% inhibition) and QR-E (8% inhibition). No difference in inhibitory potency was found between YGlapS and YEpS, both of which resulted in complete inhibition of crystal growth. The effects of phosphorylation are shown in the Supporting Information, Figure S1B. As noted above, both YGlapS and YEpS exhibited 100% inhibition of HA growth. The comparable figures for YGlaS and YES were 48% and 40%, respectively.

The results of the above-mentioned crystal-growth studies are summarized in Table 1. Taken together, the comparisons of gla-containing versus nongla-containing peptides and phosphorylated versus nonphosphorylated peptides indicate that the HA-inhibiting effect of YGlapS is increased by phosphorylation but not γ-carboxylation, while the effects of SK-Gla and QR-Gla are increased by γ-carboxylation.

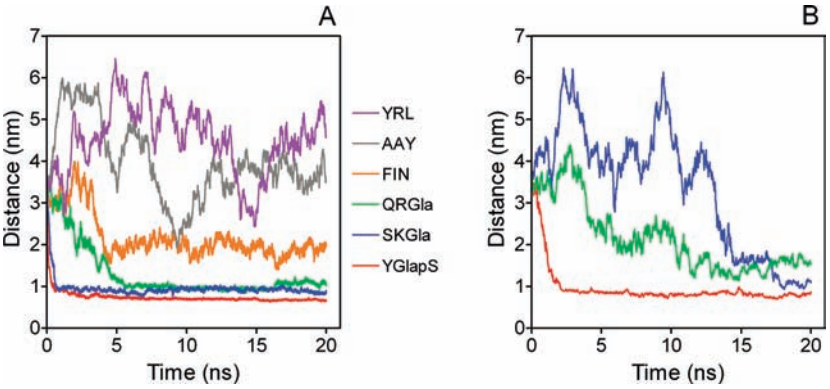

Figure 3. MD trajectory plots, native peptides. Distances between peptide centers of mass and the outermost layer of crystal atoms were calculated as described under the Experimental Section. (A) {100} face; (B) {001} face.

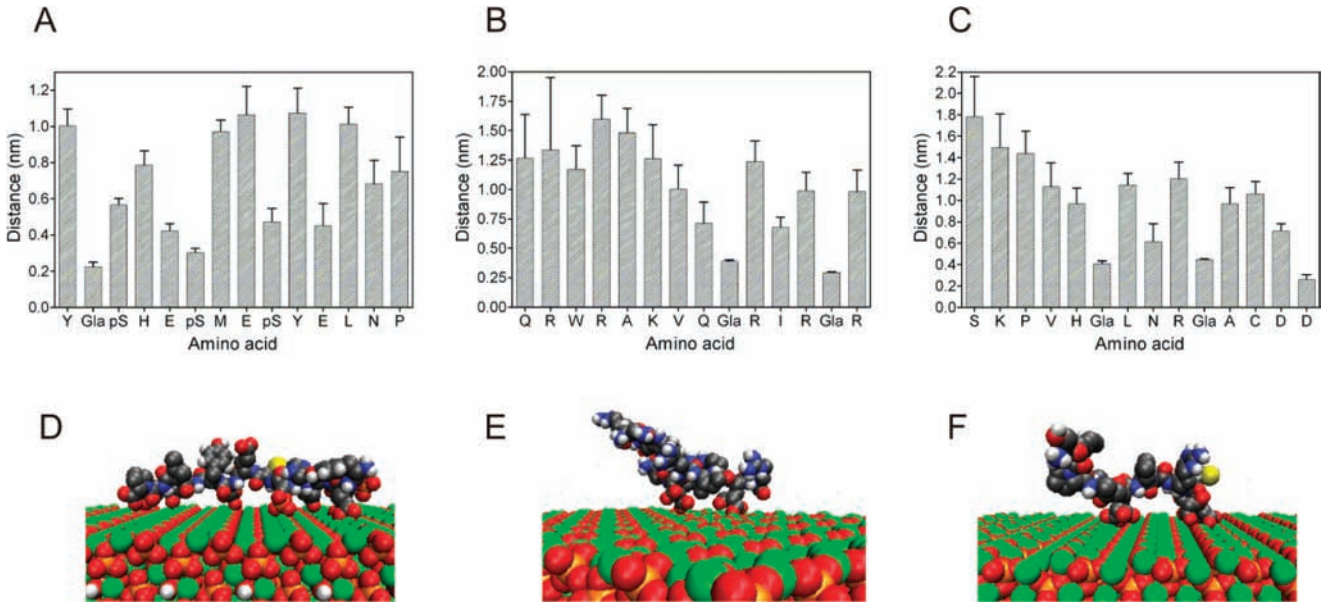

Figure 4. Amino acid center-of-mass data, {100} face. (A, B, C) Distances between amino acid centers of mass and the outermost layer of crystal atoms were averaged over 10−20 ns of simulation. Error bars represent standard deviation. (D, E, F) Snapshots of peptides at 20 ns. Color scheme: light blue = Ca; red = O; orange = P; white = H; gray = C; dark blue = N; yellow = S. (A, D) YGlapS; (B, E) QR-Gla; (C, F) SK-Gla.

Molecular Dynamics Analysis of MGP Peptide Adsorption to HA. Simulations of the 11 MGP peptides described above (YGlapS, YEpS, YGlaS, and YES; QR-Gla and QR-E; SK-Gla and SK-E; FIN, YRL, and AAY) were created. The adsorption of these virtual peptides to the {100} face of HA was studied using atomistic MD simulations. Peptide−crystal distances were calculated by measuring the peptide center-of-mass coordinate perpendicular to the surface, then subtracting the vertical position of the outer crystal surface ions. Mean and root-mean-square-deviation (rmsd) values were calculated over 10−20 ns of simulation time.

Figure 3A shows trajectory plots of the six "native" peptides. YGlapS and SK-Gla adsorb to the {100} face within the first nanosecond, and their positions do not fluctuate significantly thereafter. QR-Gla migrates more slowly toward the crystal surface, while FIN does not vary much from a distance of approximately 2 nm. The positions of YRL and AAY are essentially random. As shown in Table 1, mean peptide−crystal distances are in the order YGlapS < SK-Gla < QR-Gla < FIN < AAY < YRL. Rmsd values represent the fluctuation of the peptide's position over time and, like the mean peptide−crystal distance, should be inversely correlated with strength of adsorption. Indeed, the rmsd's of the native peptides fall in the same order as the peptide-crystal distances.

The interactions between the "non-native" virtual peptides and the {100} face were also studied. Average peptide−crystal distances are shown in Table 1. The values for YGlaS (nonphosphorylated), YEpS (non-γ-carboxylated), and YES (nonphosphorylated and non-γ-carboxylated) are only slightly higher than those for fully modified YGlapS. The peptide−crystal distances for the non-γ-carboxylated peptides SK-E and QR-E are 48% and 32%, respectively, higher than their γ-carboxylated counterparts. The differences in rmsd values are even more dramatic.

We also simulated the adsorption of the γ-carboxylated peptides YGlapS, QR-Gla, and SK-Gla to the {001} face of HA.

dx.doi.org/10.1021/ja207628k |J. Am. Chem. Soc. 2011, 133, 18406–18412

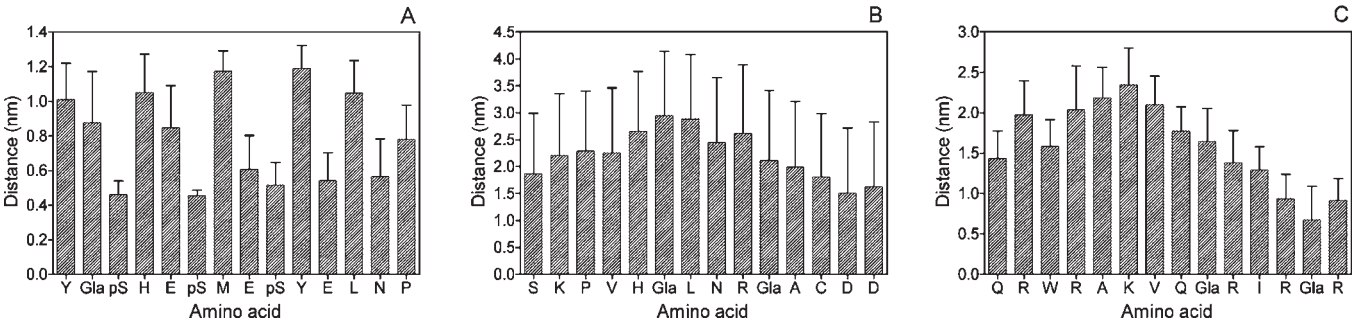

Figure 5. Amino acid center-of-mass data, {001} face. See legend to Figure 3. (A) YGlapS; (B) SK-Gla; (C) QR-Gla.

Adsorption to this face was slower than to the {100} face, but again YGlapS adsorbed most rapidly (Figure 3B). Initially, QR-Gla had a stronger tendency toward the {001} face than SK-Gla, but in the last 2.5 ns of the simulation, SK-Gla formed a closer interaction. The average peptide−crystal distances ± rmsd were as follows: YGlapS, 0.805 ± 0.048 nm; SK-Gla, 2.26 ± 1.17 nm; QR-Gla, 1.52 ± 0.231 nm. The adsorption of YGlapS to the {001} face is shown in Video 1. Note that the phosphate groups of the peptide rapidly become closely and stably associated with the crystal surface.

To identify amino acids likely to be involved in the interaction between MGP and the {100} face of HA, distances between individual side chains and the crystal surface were averaged over 10−20 ns. For YGlapS, Gla2 is the closest residue (Figure 4A). The two phosphoserines are also in close proximity to the crystal face, as are two of the three glutamic acids (E5 and E11). For SK-Gla, the two gla residues and D14 form the closest contacts (Figure 4B); for QR-Gla, the gla residues are by far the closest to the crystal surface (Figure 4C). The final positions of YGlapS, QR-Gla, and SK-Gla are shown in panels D, E, and F of Figure 4, respectively.

The adsorption of the virtual peptides YGlaS (nonphosphorylated), YEpS (non-γ-carboxylated), and YES (nonphosphorylated and non-γ-carboxylated) to the {100} face of HA was also simulated. Average side chain−crystal distances are shown in the Supporting Information, Figure S2. In the absence of the phosphoserines, E8 becomes the closest residue (Supporting Information, Figure S2A); in the absence of Gla2, pS3 is closest (Supporting Information, Figure S2B). In the absence of any post-translational modification, three of the four glutamic acids are in close contact with the crystal (Supporting Information, Figure S2C). The corresponding data for the non-γ-carboxylated peptides QR-E and SK-E are shown in the Supporting Information, Figure 3. In both cases, one of the "new" glutamic acid residues (E13 of QR-E and E10 of SK-E) is as close to the crystal as the gla residue it replaces, while the other (E9 of QR-Gla and E6 of SK-E) is much further away than the corresponding gla.

Side chain center-of-mass plots for adsorption of these peptides to the {001} face of HA are shown in Figure 5. In the case of YGlapS, the closest amino acids are pS3, pS6, pS9, and E11 (Figure 5A). Because of its slow adsorption behavior, all the amino acids of SK-Gla are relatively distant from the {001} face and have large rmsd values (Figure 5B). QR-Gla adsorbs to the {001} face primarily at the C terminus of the peptide, presumably because of Gla13 and the free carboxylate group on R14 (Figure 5C).

DISCUSSION

Atomistic MD and other simulation techniques can provide atomic-scale information about protein−crystal interactions and thus have the potential to illuminate the mechanisms by which organisms control the type, size, shape, and orientation of biominerals.[45] MD simulations have the advantage that they can resolve uncertainties and perturbations caused by, for example, probes.[46,47] In order to improve and validate computational models, it is desirable to compare the findings of simulations to physical experimentation. In past studies, we have shown, in agreement with MD analyses, that a phosphopeptide corresponding to amino acids 220−235 of rat bone osteopontin (OPN) adsorbs preferentially to the {100} faces of calcium oxalate monohydrate crystals.[33] We have also shown that the relative HA-inhibiting potencies of four OPN peptides, as shown by constant-composition analysis, are in agreement with their rates of adsorption to the {100} face of HA, as shown by MD.[34] However, the present study is the first comprehensive analysis of a protein-crystal interaction using parallel simulation and experimentation.

By using constant-composition/seeded growth, the inhibitory activities of the six "native" MGP peptides follow the series YGlapS > SK-Gla > QR-Gla > FIN > AAY > YRL. The IC_{50} value for YGlapS, 2.96 μg/mL, is similar to that previously derived for the aspartic acid-rich OPN peptide, pOPAR.[34] By using MD, the predicted order of adsorption of the MGP peptides to the {100} face of HA was exactly the same: YGlapS > SK-Gla > QR-Gla > FIN > AAY > YRL. Experimentally, it was shown that γ-carboxylation contributes to the HA-inhibiting potencies of SK-Gla and QR-Gla, while phosphorylation, but not γ-carboxylation, contributes to the potency of YGlapS; by simulation, we found the same factors affect the adsorption of these peptides to the {100} face. Although there are quantitative differences between the results obtained from the two techniques, the striking correlation gives a high level of confidence that MD provides an excellent version of physical reality.

In a previous study, synthetic γ-carboxylated peptides corresponding to amino acids 1−84, 1−53, and 35−54 of MGP were shown to inhibit the calcification of vascular smooth muscle cell (VSMC) cultures. Non-γ-carboxylated versions of these peptides had no significant activity. A phosphorylated peptide corresponding to amino acids 3−15 of MGP, but not a nonphosphorylated one, also inhibited calcification of VSMC cultures.[24] As MGP1−53 contains all five gla residues, MGP35−54 contains four of these, and MGP54−84 corresponds approximately to our peptides YRL and AAY, the effects of MGP on HA growth and smooth muscle cell calcification are very similar. Therefore,

it appears likely that the effect of MGP on VSMC calcification involves a direct interaction of the protein with nascent HA crystals.

The findings of the present study provide the first evidence for the mechanism by which MGP inhibits soft-tissue calcification in vivo. Dividing human MGP into six 14 amino acid sequences results in three peptides that are post-translationally modified and highly acidic (YGlapS, QR-Gla, and SK-Gla) and three that are not modified and weakly basic (FIN, AAY, and YRL). In agreement with our previous studies on OPN,[33,34] HA-adsorbing and -inhibiting activities are strongly correlated with acidity. Thus, SK-Gla interacts more strongly with HA than the arginine-rich QR-Gla, although the activities of both are significantly reduced by replacing the gla residues with glutamic acid. However, the single gla residue present in YGlapS had negligible effect on the HA-adsorbing and -inhibiting activities of this peptide. Phosphate groups do contribute to the interaction between YGlapS and HA, but interestingly, even the non-γ-carboxylated and nonphosphorylated versions of this peptide (YES) had stronger HA-inhibiting activity than any other peptide with the exception of SK-Gla. This is likely because YES is still quite acidic, and its even spacing of glutamic acid residues minimizes electrostatic repulsion.

Calculating distances between individual amino acids of MGP peptides and the HA crystal surface provides further insights into the role of post-translational modification in protein−crystal interactions. The amino acids in QR-Gla that are closest to the crystal surface at 10−20 ns of simulation are the two glas; in SK-Gla, the closest amino acids are the two glas and the doubly carboxylated C-terminal aspartic acid. However, consideration of the YGlapS series of peptides shows that a strong interaction can involve different combinations of anionic residues: pS6 in YGlapS but not YEpS; E11 in YEpS and YES but not YGlaS. Likewise, E10 in SK-E is closer to the crystal face than Gla10 in SK-Gla. This conclusion is also supported by comparison of the mode of interaction between YGlapS and the {100} and {001} faces. On the {100} face, Gla2 is much closer than pS3; on the {001} face, the opposite is true. However, it is clear that certain amino acids do not promote interaction with HA: large and/or nonpolar residues such as the tyrosines, methionine, and leucine of YGlapS, and basic residues such as the arginines and lysine of QR-Gla.

Little information is available on specific amino acids involved in interactions between other proteins and crystals. The three-dimensional structure of OC reveals that the three gla residues are on the same side of an α helix, with the spacing between the side-chains matching that of Ca^{2+} ions on the {100} face of HA.[48] Based on this, Capriotti et al. synthesized a gla-containing peptide designed to adopt an α-helical conformation on adsorption to mineral and showed that this peptide binds to HA with moderately high affinity.[49] The solid-state NMR technique REDOR (rotational echo double resonance) can measure distances between isotopically labeled amino acids of HA-bound proteins and nearby P atoms of the crystal.[50] By using this technique, N-terminal glutamic acid (E5) and lysine (K6) residues were shown to be involved in the adsorption of the salivary protein statherin to HA.[51,52] The involvement of both acidic and basic residues in the statherin−HA interaction was also predicted using RosettaSurface simulations.[53]

In the majority of our simulations, we have used the {100} face of HA. In hexagonal prismatic HA crystals, such as those of dental enamel, {100} is the major face developed. Bone HA crystals, in contrast, are small, irregularly shaped plates, and the faces cannot be indexed.[54] However, {100} faces have been implicated in adsorption of mineralized-tissue proteins, probably because of their high density of Ca^{2+} ions.[48,55] Therefore, we are confident that simulations involving the {100} face of HA are a good model of protein−crystal interaction. However, we have also studied the adsorption of MGP peptides to another of the principal lattice planes of HA: the {001} face, which represents the basal plane of the unit cell. Adsorption of MGP peptides to {001} is much slower than to {100}, presumably because the former face is less cationic. Nonetheless, the order of affinity of these peptides, YGlapS > SK-Gla > QR-Gla, is the same in both cases.

CONCLUSION

Parallel studies on a series of 11 MGP peptides by constant-composition autotitration and MD have provided a comprehensive validation of the use of simulation to study protein−crystal interactions. Although it may have other effects on ectopic calcification processes, MGP is a potent inhibitor of HA crystal growth. This activity involves γ-carboxylation and phosphorylation, suggesting that both the phosphorylated N terminus and the gla-containing central region participate in the interaction of MGP with HA crystals.

ASSOCIATED CONTENT

Supporting Information. Effects of post-translationally modified and nonpost-translationally modified MGP peptides on HA crystal growth (Figure S1); peptide-crystal distances for unmodified and partially modified forms of MGP1−14, MGP29−42, and MGP43−56 (Figures S2 and S3). This material is available free of charge via the Internet at http://pubs.acs.org.

Web Enhanced Feature. Video showing MD simulation of adsorption of MGP peptide YGlapS to the {001} face of HA.

AUTHOR INFORMATION

Corresponding Author
graeme.hunter@schulich.uwo.ca

Present Addresses
[§]Department of Chemistry, University of Waterloo, 200 University Avenue West, Waterloo, Ontario, N2L 3G1

ACKNOWLEDGMENT

These studies were supported by the Canadian Institutes of Health Research and the Natural Sciences and Engineering Research Council of Canada. MD simulations were made possible by the facilities of SHARCNET (www.sharcnet.ca).

REFERENCES

(1) Addadi, L.; Weiner, S.; Geva, M. *Z. Kardiol.* **2001**, *90* (Suppl 3), 92.
(2) George, A.; Veis, A. *Chem. Rev.* **2008**, *108*, 4670.
(3) Hunter, G. K.; O'Young, J.; Grohe, B.; Karttunen, M.; Goldberg, H. A. *Langmuir* **2010**, *26*, 18639.
(4) Williams, R. J. P. *Philos. Trans. R. Soc. London* **1984**, *304*, 411.
(5) Schlieper, G.; Westenfeld, R.; Brandenburg, V.; Ketteler, M. *Semin. Dial.* **2007**, *20*, 113.
(6) Ho, A. M.; Johnson, M. D.; Kingsley, D. M. *Science* **2000**, *289*, 265.

(7) Mattle, D.; Hess, B. *Urol. Res.* **2005**, *33*, 73.
(8) Kumar, V.; Lieske, J. C. *Curr. Opin. Nephrol. Hypertens.* **2006**, *15*, 374.
(9) Luo, G.; Ducy, P.; McKee, M. D.; Pinero, G. J.; Loyer, E.; Behringer, R. R.; Karsenty, G. *Nature* **1997**, *386*, 78.
(10) Price, P. A.; Williamson, M. K.; Lothringer, J. W. *J. Biol. Chem.* **1981**, *256*, 12760.
(11) Murshed, M.; Schinke, T.; McKee, M. D.; Karsenty, G. *J. Cell Biol.* **2004**, *165*, 625.
(12) Munroe, P. B.; Olgunturk, R. O.; Fryns, J. P.; Van Maldergem, L.; Ziereisen, F.; Yuksel, B.; Gardiner, R. M.; Chung, E. *Nat. Genet.* **1999**, *21*, 142.
(13) Hur, D. J.; Raymond, G. V.; Kahler, S. G.; Riegert-Johnson, D. L.; Cohen, B. A.; Boyadjiev, S. A. *Am. J. Med. Genet., Part A* **2005**, *135A*, 36.
(14) Meier, M.; Weng, L. P.; Alexandrakis, E.; Ruschoff, J.; Goeckenjan, G. *Eur. Respir. J.* **2001**, *17*, 566.
(15) Crosier, M. D.; Booth, S. L.; Peter, I.; Dawson-Hughes, B.; Price, P. A.; O'Donnell, C. J.; Hoffmann, U.; Williamson, M. K.; Ordovas, J. M. *J. Nutr. Sci. Vitaminol.* **2009**, *55*, 59.
(16) Gao, B.; Yasui, T.; Itoh, Y.; Tozawa, K.; Hayashi, Y.; Kohri, K. *J. Urol.* **2007**, *177*, 2361.
(17) Kiefer, M. C.; Bauer, D. M.; Young, D.; Hermsen, K. M.; Masiarz, F. R.; Barr, P. J. *Nucleic Acids Res.* **1988**, *16*, 5213.
(18) Price, P. A.; Rice, J. S.; Williamson, M. K. *Protein Sci.* **1994**, *3*, 822.
(19) Hackeng, T. M.; Rosing, J.; Spronk, H. M. H.; Vermeer, G. *Protein Sci.* **2001**, *10*, 864.
(20) Price, P. A.; Williamson, M. K. *J. Biol. Chem.* **1985**, *260*, 14971.
(21) Price, P. A.; Williamson, M. K.; Haba, T.; Dell, R. B.; Jee, W. S. S. *Proc. Natl. Acad. Sci.-Biol.* **1982**, *79*, 7734.
(22) Price, P. A.; Faus, S. A.; Williamson, M. K. *Arterioscler., Thromb., Vasc. Biol.* **1998**, *18*, 1400.
(23) Price, P. A. *Connect. Tissue Res.* **1989**, *21*, 381.
(24) Schurgers, L. J.; Spronk, H. M.; Skepper, J. N.; Hackeng, T. M.; Shanahan, C. M.; Vermeer, C.; Weissberg, P. L.; Proudfoot, D. *J. Thromb. Haemostasis* **2007**, *5*, 2503.
(25) Yagami, K.; Suh, J. Y.; Enomoto-Iwamoto, M.; Koyama, E.; Abrams, W. R.; Shapiro, I. M.; Pacifici, M.; Iwamoto, M. *J. Cell Biol.* **1999**, *147*, 1097.
(26) Romberg, R. W.; Werness, P. G.; Riggs, B. L.; Mann, K. G. *Biochemistry* **1986**, *25*, 1176.
(27) Hunter, G. K.; Hauschka, P. V.; Poole, A. R.; Rosenberg, L. C.; Goldberg, H. A. *Biochem. J.* **1996**, *317*, 59.
(28) Long, J. R.; Dindot, J. L.; Zebroski, H.; Kihne, S.; Clark, R. H.; Campbell, A. A.; Stayton, P. S.; Drobny, G. P. *Proc. Natl. Acad. Sci. U.S.A.* **1998**, *95*, 12083.
(29) Roy, M. E.; Nishimoto, S. K. *Bone* **2002**, *31*, 296.
(30) Price, P. A.; Thomas, G. R.; Pardini, A. W.; Figueira, W. F.; Caputo, J. M.; Williamson, M. K. *J. Biol. Chem.* **2002**, *277*, 3926.
(31) Doherty, T. M.; Asotra, K.; Fitzpatrick, L. A.; Qiao, J. H.; Wilkin, D. J.; Detrano, R. C.; Dunstan, C. R.; Shah, P. K.; Rajavashisth, T. B. *Proc. Natl. Acad. Sci. U.S.A.* **2003**, *100*, 11201.
(32) Bostrom, K.; Tsao, D.; Shen, S.; Wang, Y.; Demer, L. L. *J. Biol. Chem.* **2001**, *276*, 14044.
(33) Grohe, B.; O'Young, J.; Ionescu, A.; Lajoie, G.; Rogers, K. A.; Karttunen, M.; Goldberg, H. A.; Hunter, G. K. *J. Am. Chem. Soc.* **2007**, *129*, 14946–14951.
(34) Azzopardi, P. V.; O'Young, J.; Lajoie, G.; Karttunen, M.; Goldberg, H. A.; Hunter, G. K. *PLos One* **2010**, *5*, e9330.
(35) Van Der Spoel, D.; Lindahl, E.; Hess, B.; Groenhof, G.; Mark, A. E.; Berendsen, H. J. *J. Comput. Chem.* **2005**, *26*, 1701.
(36) Schuler, L. D.; Daura, X.; van Gunsteren, W. F. *J. Comput. Chem.* **2001**, *22*, 1205.
(37) Berendsen, H. J. C., Postma, J. P. M., van Gunsteren, W. F., Hermans, J. In *Intermolecular Forces*; Pullman, B., Ed.; Reidel: Dordrecht, Netherlands, 1981.
(38) Patra, M.; Karttunen, M. *J. Comput. Chem.* **2004**, *25*, 678.
(39) Ryckaert, J. P.; Ciccotti, G.; Berendsen, H. J. C. *J. Comput. Phys.* **1977**, *23*, 327.
(40) Darden, T.; York, D.; Pedersen, L. *J. Chem. Phys.* **1993**, *98*, 10089.
(41) Karttunen, M.; Rottler, J.; Vattulainen, I.; Sagui, C. *Curr. Top. Membr.* **2008**, *60*, 49.
(42) Patra, M.; Karttunen, M.; Hyvonen, M. T.; Lindqvist, P.; Falck, E.; Vattulainen, I. *Biophys. J.* **2003**, *84*, 3636.
(43) van der Spoel, D.; van Maaren, P. J. *J. Chem. Theory Comput.* **2006**, *2*, 1.
(44) Wong-Ekkabut, J.; Miettinen, M. S.; Dias, C.; Karttunen, M. *Nat. Nanotechnol.* **2010**, *5*, 555.
(45) Harding, J. H.; Duffy, D. M.; Sushko, M. L.; Rodger, P. M.; Quigley, D.; Elliott, J. A. *Chem. Rev.* **2008**, *108*, 4823.
(46) Repakova, J.; Holopainen, J. M.; Karttunen, M.; Vattulainen, I. *J. Phys. Chem. B* **2006**, *110*, 15403.
(47) Stimson, L.; Dong, L.; Karttunen, M.; Wisniewska, A.; Dutka, M.; Rog, T. *J. Phys. Chem. B* **2007**, *111*, 12447.
(48) Hoang, Q. Q.; Sicheri, F.; Howard, A. J.; Yang, D. S. *Nature* **2003**, *425*, 977.
(49) Capriotti, L. A.; Beebe, T. P., Jr.; Schneider, J. P. *J. Am. Chem. Soc.* **2007**, *129*, 5281.
(50) Drobny, G. P.; Goobes, G.; Stayton, P. S. *Prog. Nucl. Magn. Reson. Spectrosc.* **2007**, *50*, 71.
(51) Ndao, M.; Ash, J. T.; Breen, N. F.; Goobes, G.; Stayton, P. S.; Drobny, G. P. *Langmuir* **2009**, *25*, 12136.
(52) Raghunathan, V.; Gibson, J. M.; Goobes, G.; Popham, J. M.; Louie, E. A.; Stayton, P. S.; Drobny, G. P. *J. Phys. Chem. B* **2006**, *110*, 9324.
(53) Masica, D. L.; Gray, J. J. *Biophys. J.* **2009**, *96*, 3082.
(54) Weiner, S.; Price, P. A. *Calcif. Tissue Int.* **1986**, *39*, 365.
(55) Fujisawa, R.; Kuboki, Y. *Biochim. Biophys. Acta* **1991**, *1075*, 56.